Acta Oceanol. Sin., 2021, Vol. 40, No. 10, P. 49–64
https://doi.org/10.1007/s13131-021-1831-1
http://www.aosocean.com
E-mail: ocean2@hyxb.org.cn

Impacts of human interventions on the seasonal and nodal dynamics of the M_2 and K_1 tidal constituents in Lingdingyang Bay of the Zhujiang River Delta, China

Ping Zhang[1, 2, 3], Qingshu Yang[1, 2, 3], Haidong Pan[4], Heng Wang[1, 2, 3], Meifang Xie[1, 2, 3], Huayang Cai[1, 2, 3]*, Nanyang Chu[5], Liangwen Jia[1, 2, 3]

[1] Institute of Estuarine and Coastal Research, School of Marine Engineering and Technology, Sun Yat-sen University, Zhuhai 519082, China

[2] Guangdong Provincial Engineering Research Center of Coasts, Islands and Reefs, Zhuhai 519082, China

[3] Southern Marine Science and Engineering Guangdong Laboratory (Zhuhai), Zhuhai 519080, China

[4] Key Laboratory of Physical Oceanography, Ministry of Education, Qingdao 266100, China

[5] School of Marine Science, Sun Yat-sen University, Zhuhai 519082, China

Received 3 November 2020; accepted 28 February 2021

Abstract

Natural and human-induced changes may exert considerable impacts on the seasonal and nodal dynamics of M_2 and K_1 tidal constituents. Therefore, quantifying the influences of these factors on tidal regime changes is essential for sustainable water resources management in coastal environments. In this study, the enhanced harmonic analysis was applied to extract the seasonal variability of the M_2 and K_1 tidal amplitudes and phases at three gauging stations along Lingdingyang Bay of the Zhujiang River Delta. The seasonal dynamics in terms of tidal wave celerity and amplification/damping rate were used to quantify the impacts of human-induced estuarine morphological alterations on M_2 and K_1 tidal hydrodynamics in inner and outer Lingdingyang Bay. The results show that both tidal amplification/damping rate and wave celerity were considerably increased from the pre-anthropogenic activity period (Pre-AAP) to the post-anthropogenic activity period (Post-AAP) excepting the tidal amplification/damping rate in outer Lingdingyang Bay, and the variations in outer Lingdingyang Bay was larger than those in inner Lingdingyang Bay. The alterations in these two parameters were more significant in flood season than in dry season in both inner and outer Lingdingyang Bay. The seasonal variability of M_2 and K_1 tidal amplitudes were further quantified using a regression model accounting for the 18.61-year lunar nodal modulation, where this study observes a considerable alteration in M_2 constituent owing to human interventions. During the Post-AAP, the M_2 amplitudes at the downstream station were larger than those that would have occurred in the absence of strong human interventions, whereas the opposite was true for the upstream station, leading to a substantial decrease in tidal amplification in outer Lingdingyang Bay. However, it is opposite in inner Lingdingyang Bay. The underlying mechanism can be primarily attributed to channel deepening and narrowing caused by human interventions, that resulted in substantial enlargement of the bay volume and reduced the effective bottom friction, leading to faster wave celerity and stronger amplified waves.

Key words: tidal dynamics, S_TIDE model, nodal modulation, channel deepening, tidal wave celerity

Citation: Zhang Ping, Yang Qingshu, Pan Haidong, Wang Heng, Xie Meifang, Cai Huayang, Chu Nanyang, Jia Liangwen. 2021. Impacts of human interventions on the seasonal and nodal dynamics of the M_2 and K_1 tidal constituents in Lingdingyang Bay of the Zhujiang River Delta, China. Acta Oceanologica Sinica, 40(10): 49–64, doi: 10.1007/s13131-021-1831-1

1 Introduction

It is essential to understand tidal variability in coastal areas because it directly impacts channel navigation, coastal flooding, and ecology. Previous studies examining tidal dynamics have shown that tidal fluctuations occur over a wide range of time scales (including sub-daily, daily, fortnightly, seasonal, yearly, and decadal) owing to the changes in predictable astronomical variations and the physical properties of the ocean and coastal morphology (Devlin et al., 2014, 2017, 2018). This study mainly focuses on the seasonal variability of tides, which is significant in the Zhujiang River Delta (ZRD) located in the southern part of China. Of particular interest are the impacts of large-scale human interventions on the seasonal variability of tides.

Seasonal variability of the main tidal constituents has been documented for a long time (Corkan, 1934; Kang et al., 1995; Gräwe et al., 2014; Müller et al., 2014). In the coastal ocean, it is usually observed that tidal amplitudes are larger during summer than during winter (Huess and Andersen, 2001; Tazkia et al., 2017; Wang et al., 2020a). This can be primarily attributed to the seasonal variation in frictional effects exerted on tides when they propagate from the deep ocean to the open area of the coastal ocean. In contrast, in the inner parts of the delta, amplitudes of

Foundation item: The National Key R&D Program of China under contract No. 2016YFC0402600; the National Natural Science Foundation of China under contract No. 51979296; the Guangzhou Science and Technology Program of China under contract No. 202002030452.

*Corresponding author, E-mail: caihy7@mail.sysu.edu.cn

the main tidal constituents are relatively large during winter and smaller during summer, mainly due to seasonal changes in river discharge (Godin, 1985, 1999; Guo et al., 2015; Cai et al., 2016; Pan et al., 2018a). Many previous studies have addressed the seasonal variability of tidal characteristics in coastal areas accounting for the impacts of natural changes in sea level dynamics (Devlin et al., 2017), stratification (Müller, 2012), and sea ice dynamics (St-Laurent et al., 2008). However, the impacts of human interventions (e.g., land reclamation, dredging for navigational channels, and sand excavation) on the seasonal variability of tidal dynamics have received little attention yet.

In this contribution, water level observations at three gauging stations along Lingdingyang Bay of the ZRD were used to explore the seasonal variability of the dominant tidal constituents (i.e., M_2 and K_1) by means of enhanced harmonic analysis (EHA). The paper is organized as follows. Section 2 describes the EHA method to extract the monthly tidal amplitudes and phases. An overview of Lingdingyang Bay is provided in Section 3. In Section 4, the seasonal variability of the dominant M_2 and K_1 constituents is analyzed, and the impacts of human interventions on tidal dynamics in terms of tidal amplification/damping rate and wave celerity are discussed. Finally, the conclusions drawn are presented in Section 6.

2 Methodology and data

2.1 *Enhanced harmonic analysis model*

The EHA (Jin et al., 2018) was adapted in this study, which is based on a cubic spline interpolation and an independent point (IP) scheme, to extract time-varying harmonic parameters of main constituents. To implement EHA, Pan et al. (2018b) developed the S_TIDE MATLAB toolbox (available from https://www.researchgate.net/project/A-non-stationary-tidal-analysis-toolbox-S-TIDE) from the widely-used T_TIDE toolbox (Pawlowicz et al., 2002). In the newly developed EHA, it is assumed that the time-varying water levels can be described by the following expression:

$$Z(t) = S(t) + \sum_{j=1}^{N} [a_j(t)\cos\sigma_j t + b_j(t)\sin\sigma_j t], j = 1, \cdots, N, \quad (1)$$

where $Z(t)$ is the water level at time t, $S(t)$ represents the mean water level (MWL); and σ_j, a_j, and b_j are the frequency, cosine amplitude, and sine amplitude corresponding to the jth tidal constituent, respectively. The time-varying $S(t)$ and tidal coefficients $a_j(t)$ and $b_j(t)$ can be expressed by functions of S_i, $a_{i,j}$, and $b_{i,j}$:

$$S(t) = \sum_{i=1}^{M_S} f_{t,i}S_i, \quad a_j(t) = \sum_{j=1}^{M} f_{t,i}a_{i,j}, \quad b_j(t) = \sum_{j=1}^{M} f_{t,i}b_{i,j}, \quad (2)$$

where $f_{t,i}$ is the interpolation weight for the ith IP at time t, which depends on the interpolation method; M_S and M are the IP numbers for the MWL and tidal constituents, respectively. Combination of Eqs (1) and (2) yields:

$$Z(t) = \sum_{i=1}^{M} f_{t,i}S_i + \sum_{j=1}^{N}\left(\sum_{j=1}^{M} f_{t,i}a_{i,j}\cos\sigma_j t + \sum_{j=1}^{M} f_{t,i}b_{i,j}\sin\sigma_j t\right), \quad (3)$$

where S_i, $a_{i,j}$, and $b_{i,j}$ can be extracted through the least squares method (see details in Pan et al., 2018b). Therefore, time-varying $S(t)$, $a_j(t)$, and $b_j(t)$ can be obtained by Eq. (2). Finally, the time-varying amplitude η and phase ϕ can be computed by the following equations:

$$\eta_j = \sqrt{{a_j}^2 + {b_j}^2}, \ \phi_j = \arctan\frac{b_j}{a_j}. \quad (4)$$

2.2 *Lunar constituent modulation model*

The harmonic parameters of 18.61-year nodal modulation and the long-term linear trend can be estimated by a regression model, which can be expressed as follows (Pan et al., 2019):

$$H(t) = \beta_1 + \beta_2 t + \alpha_1\cos\left(\frac{2\pi}{18.61}t\right) + \alpha_2\sin\left(\frac{2\pi}{18.61}t\right), \quad (5)$$

where $H(t)$ is the estimated amplitude of the studied constituent (M_2 or K_1) extracted by the least square method at time t (in units of years), β_1 is a constant value, β_2 is the linear trend, and α_1 and α_2 are the amplitudes of the cosine and sine functions of the nodal cycle. Subsequently, the amplitude of 18.61-year lunar nodal modulation can be calculated as:

$$\eta_{18.61\text{-year}} = \sqrt{{\alpha_1}^2 + {\alpha_2}^2}. \quad (6)$$

2.3 *Data*

In this study, daily high and low water level time series (1965–2016) from three gauging stations were collected, including Hong Kong (denoted by HK), Chiwan (denoted by CW) and Sishengwei (denoted by SSW), along Lingdingyang Bay of the ZRD. Here, the water level time series in CW and SSW stations were collected from the hydrological data of the Zhujiang River Basin, and those in HK station were collected from the University of Hawaii Sea Level Center (UHSLC, https://uhslc.soest.hawaii.edu/, Caldwell et al., 2015). The water level observations in CW and SSW stations were corrected to the local Zhujiang River Datum. Based on the extracted tidal harmonics using EHA model, the tidal wave celerity of the tidal constituent (denoted as c) can be estimated using the following formula:

$$c = \frac{\Delta x}{(\phi_2 - \phi_1)\,T/360}, \quad (7)$$

where Δx is the distance between two adjacent stations, ϕ_1 and ϕ_2 are the phases extracted from the downstream and upstream station, respectively, and T is the period of the dominant M_2 or K_1 constituent.

The tidal wave amplitude amplification/damping rate (denoted as δ) can be defined as:

$$\delta = \frac{1}{(\eta_1 + \eta_2)/2}\frac{\eta_2 - \eta_1}{\Delta x}, \quad (8)$$

where η_1 and η_2 are the tidal constituent amplitudes extracted from the downstream and upstream station, respectively. When δ>0 (i.e., η_2>η_1), the tidal wave amplitude increases along the channel and represents the amplification rate. In contrast, δ<0 (i.e., η_2<η_1) represents the damping rate with decreasing tidal

wave amplitude along the channel.

To identify the bathymetry changes and their different impacts on tidal hydrodynamics in inner and outer Lingdingyang Bay, bathymetric maps of Lingdingyang Bay in 1965, 1998, and 2014 were collected from the Guangzhou Maritime Safety Administration and the China People's Liberation Army Navy Command Assurance Department of Navigation to explore the erosion and siltation patterns in Lingdingyang Bay. Here, the digital elevation model (DEM) of Lingdingyang Bay was generated based on digitalized isobaths and coastal lines. The bathymetric data (converted from the local lowest tidal level to the local Zhujiang River Datum) were projected to UTM-WGS84 coordinates of China and interpolated to a 50 m×50 m grid DEM in the ArcGIS software.

3 Study area

The Lingdingyang Bay is the largest bell-shaped convergent estuary in the ZRD (Fig. 1a), which consists of three shoals (the West Shoal, Middle Shoal, and East Shoal) and two channels (the West Channel and East Channel). It mainly originates from the North River and East River and flows into the South China Sea through Humen, Jiaomen, Hongqimen, and Hengmen. As a densely urbanized and populated region, Lingdingyang Bay is subject to large-scale human interventions. The evolution of the morphology of Lingdingyang Bay was mainly governed by natural processes before the 1980s, after which human activities (e.g., channel degradation and reclamation projects) have dramatically modified the bay's morphology. It was shown that the net accretion rate of the subaqueous delta in the Lingdingyang Bay decreased from 16.6 mm/a between 1955 and 1964 to 1.6 mm/a in the period of 1998–2008 because of a dramatic decline in the suspended sediment load (Wu et al., 2016b). In addition, nearly 200 km^2 of the shallow coastal area was reclaimed from 1988 to 2008 (Wu et al., 2014), and continuous dredging and a surge of sand excavation resulted in local changes in a water depth of ±5 m/a between 2012 and 2013, which far exceed the magnitude of natural topographic evolution in the Lingdingyang Bay (Wu et al., 2016a). It was shown that the tidal prism and energy dissipation rate in the Lingdingyang Bay has decreased by approximately 14.11% and 23% from 1906 to 2014, respectively (Zhou et al., 2016), which indicates a reduction in tidal energy entering into the bay. However, due to the enlargement of the bay volume and hence the reduction of the effective bottom friction, this study observes considerable increases in both tidal amplification and wave celerity. The tides coming from the Pacific Ocean propagate through the Luzon Strait into the ZRD with a mean tidal range between 1.0 m and 1.7 m (1.69 m at Humen) (Ye and Preiffer, 1990; Mao et al., 2004) and are characterized by an irregular and semidiurnal character. This study focuses on the seasonal variability of tidal dynamics in terms of tidal wave celerity and tidal amplification/damping rate estimated from three gauging stations (HK, CW, and SSW, see their locations in Fig. 1b) in the Lingdingyang Bay.

4 Results

4.1 *Tidal regime shift in Lingdingyang Bay*

The monthly variations of the M_2 and K_1 constituents tides extracted by the EHA model are shown in Fig. 2, where five independent points were used for the M_2 and K_1 constituents while the harmonic parameters of other tidal constituents were assumed to be constant (Wang et al., 2020a). Figures 2a and b show that the monthly averaged M_2 and K_1 amplitudes at HK, CW and SSW stations both had 18.61-year periodic oscillations. The amplitude of seaward station (HK) for M_2 is smaller than that in the landward station (SSW) while for K_1 constituent in CW station was more or less the same as that in SSW station. Figures 2c and d show that the phases at the three gauging stations all declined from 1965 to 2016. It should be noted that the fluctuation of phases for the M_2 constituent at SSW station was larger (from 0° to –22°) than those at CW station (decreased from –70° to –78°) and HK station (from –100° to –98°). Notably, the phases for K_1 constituent had a significant 18.61-year periodic oscillation (Fig. 2d), which is rather different from M_2 constituent (Fig. 2c). Specifically, this has to do with the fact that the impact of lunar nodal modulation for different constituents depends on their frequencies. Previous studies showed that the nodal angle (u) for long-term modulations of phase for M_2 and N_2 constituents are

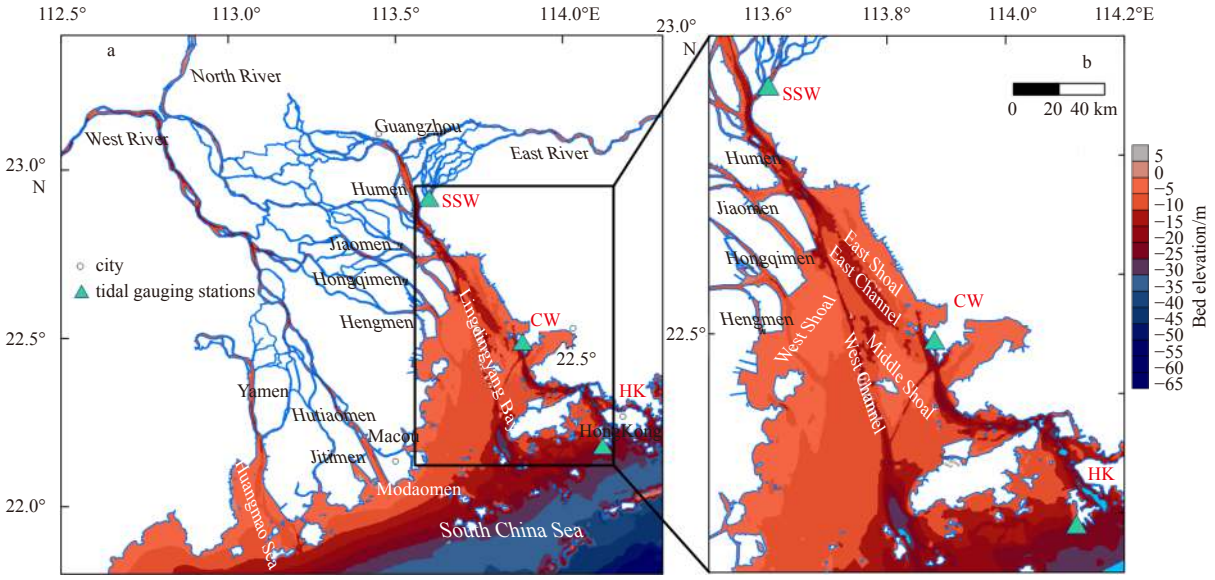

Fig. 1. Map of Lingdingyang Bay in the Zhujiang River Delta (ZRD) connected with the South China Sea (a) and the locations of the Hong Kong (HK), Chiwan (CW), and Sishengwei (SSW) gauging stations (b).

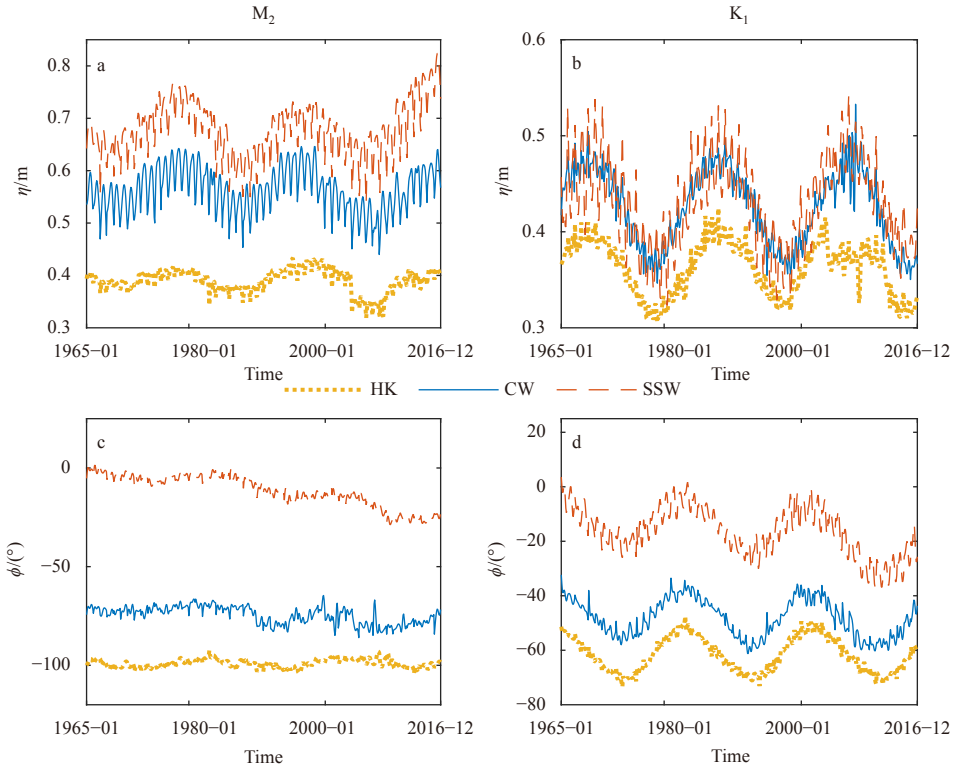

Fig. 2. Temporal variations in monthly averaged amplitudes (a, b) and phases (c, d) extracted from EHA model for the M_2 and K_1 constituents at Hong Kong (HK), Chiwan (CW), and Sishengwei (SSW) stations.

much smaller (–2.1°) than O_1 constituent (10.8°) and K_1 constituent (–8.9°) (Pugh and Woodworth, 2014; Feng et al., 2015). For more details about the definitions of nodal factor (f) and nodal angle (u), readers can refer to Eq. (S1) in the Supplementary information.

Based on Eqs (7) and (8), the tidal wave celerity c and tidal amplification/damping rate δ between HK, CW and SSW stations were calculated. The results are shown in Fig. 3. For the M_2 constituent, it was shown in Fig. 3a that the tidal amplification rate δ (where δ>0) decreased slightly for the first half period and then increased abruptly until 2016 both in the inner (from CW station to SSW station) and the outer Lingdingyang Bay (from HK station to CW station), which suggests that the tidal hydrodynamics became stronger during the study period. More specifically, it is notable that δ in outer Lingdingyang Bay (the value of δ increased from 6.2×10^{-6} m^{-1} to 7.8×10^{-6} m^{-1}) was much larger than that in inner Lingdingyang Bay (the value of δ increased from 3.2×10^{-6} m^{-1} to 4.5×10^{-6} m^{-1}). For the K_1 constituent, the tidal amplification δ in outer Lingdingyang Bay had a fluctuation change in the study period (shown in Fig. 3b), where it declined from 3.6×10^{-6} m^{-1} to 2.4×10^{-6} m^{-1}, while in inner Lingdingyang Bay it was between -2×10^{-6} m^{-1} and 2×10^{-6} m^{-1} with a rising tendency, which also suggests enhanced tidal hydrodynamics. It can be seen from Fig. 3c that the tidal wave celerity c in outer Lingdingyang Bay notably fluctuated in the study periods, but it generally inclined to 15 m/s in 2016, while in the inner Lingdingyang Bay it increased slightly from 6.8 m/s until 1994 and then inclined abruptly to 9.8 m/s in 2016. For the K_1 constituent, the tidal wave celerity c performed similarly with M_2 although the phases had significant 18.61-year periodic oscillations (Fig. 3d).

To identify the seasonal variation of tidal hydrodynamics in the Lingdingyang Bay, this study used the accumulated anomaly curve method to explore the abrupt shift year of tidal wave celerity c of M_2 and K_1 constituents during 1965–2016. Accumulated anomaly curve is a simple yet effective approach for identifying change-point of the examined time series (Wei, 2007). In this approach, for given the time series x_i, the accumulated anomaly at moment t is defined as

$$S_t = \sum_{i=1}^{n} (x_i - \bar{x}), \ i = 1, \cdots, n, \tag{9}$$

where $\bar{x} = 1/n \cdot \sum x_i$ is the mean value of the time series. Here, the temporal variation of S_t at N moments can be used to detect the change-point where the gradient with respect to the time is zero. As shown in Fig. 4, the tidal wave celerity c shift for M_2 and K_1 constituents occurred in 1990 and 2000 in outer Lingdingyang Bay, respectively, while it occurred in 1994 and 1998, respectively, in inner Lingdingyang Bay. It could be seen from Figs 2a and b that the mean tidal amplitudes for the M_2 constituent were 0.39 m, 0.56 m, and 0.67 m in HK, CW, and SSW stations, respectively, which were larger than those for the K_1 constituent (0.36 m, 0.42 m, and 0.43 m, respectively). Therefore, the shifted year based on the accumulated curve of the dominant M_2 constituent in the Lingdingyang Bay can be determined. Subsequently, this study divided the study period into two sub-periods depend on the shift period of M_2 constituent: the Pre-AAP (1965–1990 in outer Lingdingyang Bay and 1965–1994 in inner Lingdingyang Bay) with mostly natural development and the Post-AAP (1991–2016 in outer Lingdingyang Bay and 1995–2016 in inner Lingdingyang Bay) with strong human-induced modification.

Figure 5 shows that seasonal fluctuations of tidal wave celerity c and tidal amplification/damping rate δ for M_2 and K_1 con-

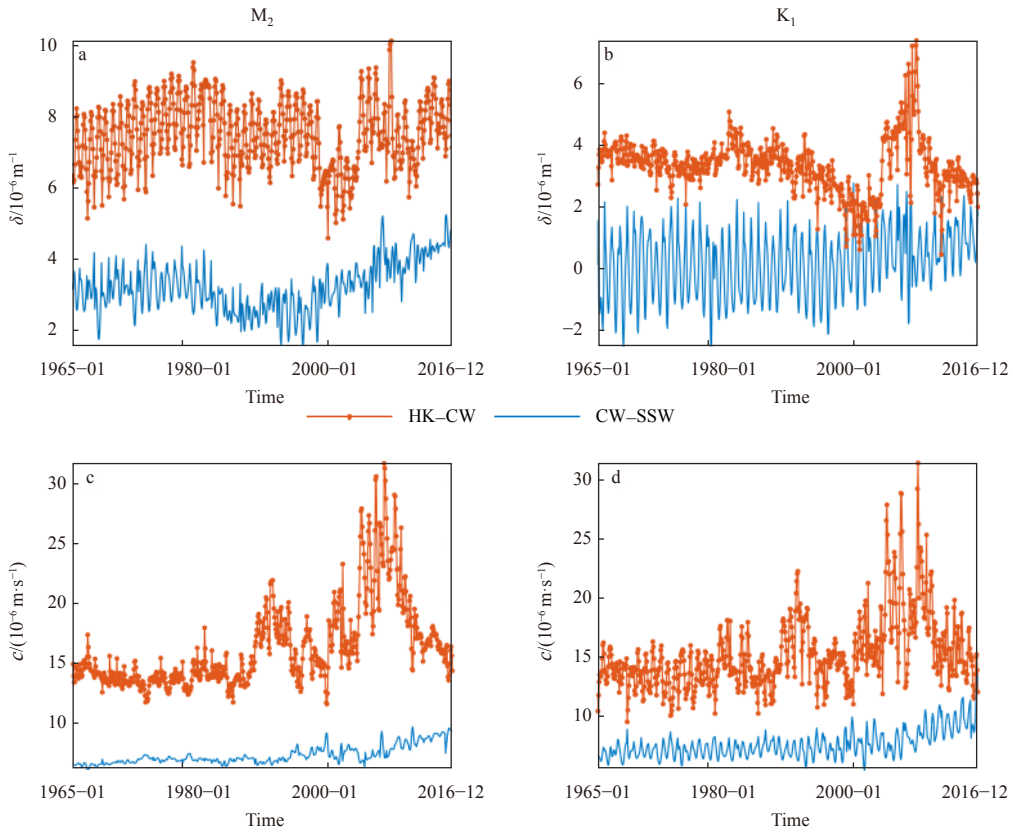

Fig. 3. Temporal variations in monthly averaged tidal amplification/damping rate δ (a, b) and wave celerity c (c, d) observed in inner (CW-SSW) and outer (HK-CW) Lingdingyang Bay.

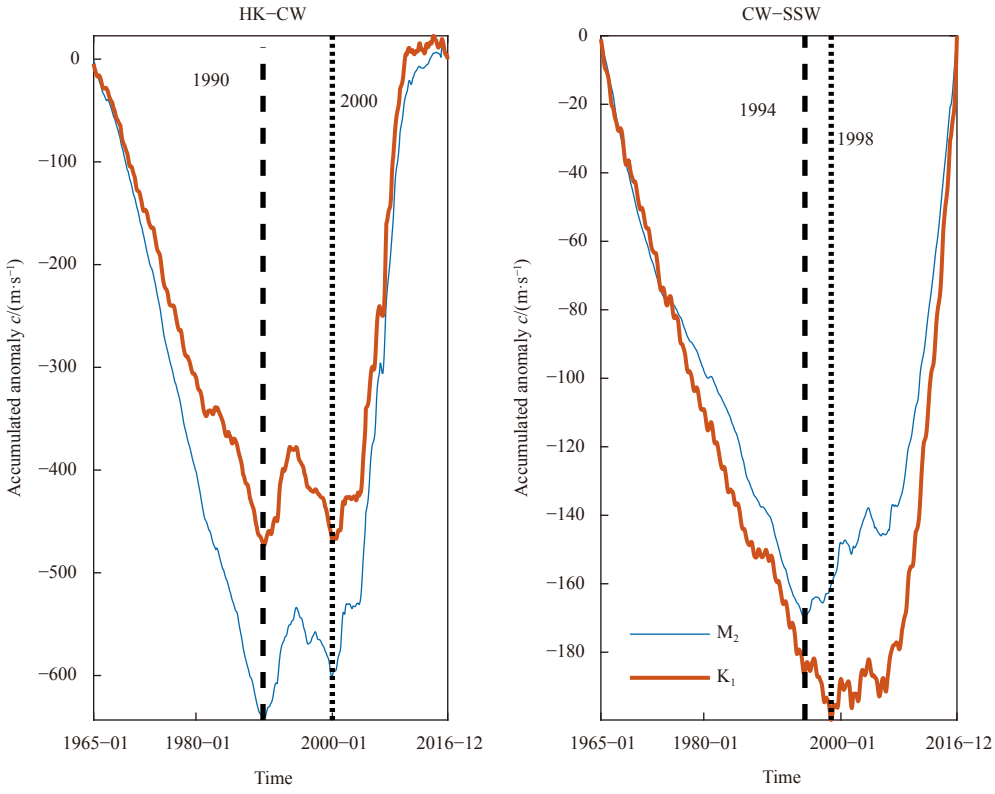

Fig. 4. Accumulated anomaly curve of the monthly averaged tidal wave celerity c of M_2 and K_1 constituents observed in inner (CW-SSW) and outer (HK-CW) Lingdingyang Bay. The dashed lines represent the change year when the c value abruptly shifted.

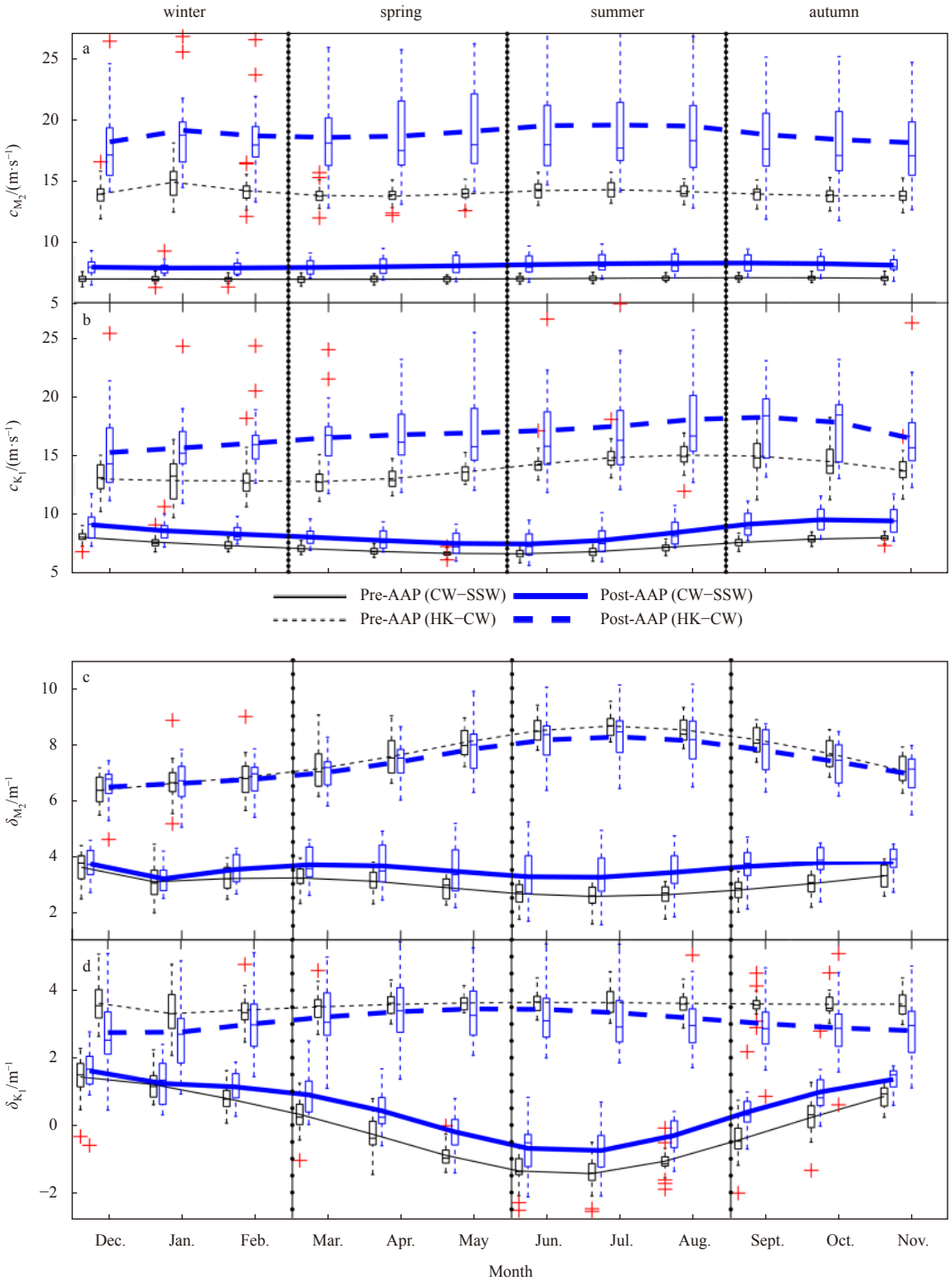

Fig. 5. Monthly averaged tidal wave celerity c (a, b) and tidal amplification/damping rate δ (c, d) distributions for both Pre-AAP and Post-AAP in inner (CW–SSW) and outer (HK–CW) Lingdingyang Bay. The black and blue lines represent the temporal variations in the mean value for the Pre-AAP and Post-AAP, respectively. The "+" symbol represents the outlier.

stituents in inner and outer Lingdingyang Bay during the Pre-AAP and Post-AAP, where increases in c and δ (representing faster tidal wave propagation and a weaker tidal damping effect) after significant human interventions were observed for four seasons. It is shown in Figs 5a and b that the values of c for the M_2 constituent were more sensitive to human interventions during spring and summer than those during winter and autumn in inner and outer Lingdingyang Bay (based on the seasonal average value of changing rate). Concerning the K_1 constituent, it is observed that the values of c were more sensitive in summer and autumn than winter and spring in inner Lingdingyang Bay while the case was converse in outer Lingdingyang Bay. To be more specific, the occurrence of maximum c for the M_2 constituent in outer Lingdingyang Bay changed from January during Pre-AAP (14.87 m/s) to July during Post-AAP (19.54 m/s) owing to human interventions (Table 1). On the other hand, it can be seen from

Table 1. Monthly averaged tidal wave celerity c distributions for both the Pre-AAP and Post-AAP in inner (CW–SSW) and outer (HK–CW) Lingdingyang Bay and the change ratio when these two periods were compared

Season	Month	HK–CW						CW–SSW					
		Pre-AAP c/(m·s^{-1})		Post-AAP c/(m·s^{-1})		Ratio/%		Pre-AAP c/(m·s^{-1})		Post-AAP c/(m·s^{-1})		Ratio/%	
		M_2	K_1	M_2	K_1	M_2	K_1	M_2	K_1	M_2	K_1	M_2	K_1
Winter	Dec.	13.91	12.94	18.16	15.21	30.61	17.50	6.96	7.95	7.93	9.03	13.84	13.50
	Jan.	14.87	12.80	19.10	15.60	28.49	21.87	6.96	7.55	7.86	8.52	12.92	12.87
	Feb.	14.18	12.78	18.66	16.01	31.64	25.23	6.94	7.25	7.86	8.24	13.26	13.63
Spring	Mar.	13.79	12.71	18.53	16.47	34.40	29.57	6.93	7.00	7.90	7.97	13.92	13.89
	Apr.	13.72	12.98	18.64	16.72	35.81	28.88	6.94	6.77	7.96	7.68	14.76	13.52
	May	13.92	13.53	19.04	16.88	36.80	24.80	6.95	6.59	8.04	7.43	15.65	12.83
Summer	Jun.	14.17	14.21	19.49	17.09	37.52	20.21	6.98	6.55	8.13	7.38	16.49	12.75
	Jul.	14.26	14.75	19.54	17.46	37.07	18.36	7.01	6.72	8.20	7.69	17.01	14.43
	Aug.	14.11	14.98	19.45	18.03	37.79	20.38	7.04	7.09	8.25	8.35	17.15	17.82
Autumn	Sept.	13.90	14.90	18.75	18.21	34.88	22.27	7.06	7.51	8.26	9.07	17.01	20.82
	Oct.	13.77	14.43	18.35	17.77	33.30	23.15	7.06	7.80	8.21	9.45	16.39	21.11
	Nov.	13.77	13.68	18.10	16.39	31.46	19.83	7.02	7.92	8.09	9.36	15.20	18.09

Fig. 5b the occurrence of maximum c for the K_1 constituent in outer Lingdingyang Bay changed from August during Pre- AAP (14.98 m/s) to September during Post-AAP (18.21 m/s). In inner Lingdingyang Bay, the occurrence of maximum c for M_2 and K_1 constituents changed both from September to October (increased from 7.06 m/s to 8.26 m/s, from 7.80 m/s to 9.45 m/s, respectively). Similar to tidal wave celerity, the values of δ were more sensitive to human interventions during spring and summer than during winter and autumn in inner Lingdingyang Bay, while it was contrast in outer Lingdingyang Bay (shown in Figs 5c and d). The maximum values of δ occurred in the same month for the M_2 constituent (i.e., in July and the values are 8.64×10^{-6} m^{-1} and 8.26×10^{-6} m^{-1}, respectively) in both Pre-AAP and Post-AAP, but for the K_1 constituent it occurred in June and May (decreased from 3.64×10^{-6} m^{-1} and 3.45×10^{-6} m^{-1}, respectively) in outer Lingdingyang Bay (Table 2). While in inner Lingdingyang Bay, the maximum value of δ occurred in the same month for M_2 and K_1 (i.e., in November and the values are 3.59×10^{-6} m^{-1} and 1.43×10^{-6} m^{-1}, respectively) during Pre-AAP while those for M_2 and K_1 constituents occurred in November (3.79×10^{-6} m^{-1}) and December (1.61×10^{-6} m^{-1}) during Post-AAP, respectively. The variations of these two parameters in terms of ratio were also calculated, and the results are shown in Tables 1 and 2, respectively. The average variations of c and δ in spring and summer were stronger than those in winter and autumn in both inner and outer Lingdingyang Bay, which is likely due to the large freshwater discharge debouched from the upstream ZRD. Overall, the results suggest that due to human interventions more considerable changes of tidal amplification/damping rate δ occurred in inner Lingdingyang Bay than those in outer Lingdingyang Bay. On the contrary, it was observed that the changes in tidal wave celerity c were more considerable in outer Lingdingyang Bay than those in inner Lingdingyang Bay.

4.2 *Nodal modulation of the M_2 and K_1 constituents*

It is shown in Fig. 2 that the M_2 and K_1 amplitudes at all HK, CW, and SSW stations had apparent 18.61-year periodic variations during Pre-AAP and Post-AAP. Thus, a regression model adopting Eq. (5) was used to extract the fitting curves (representing the nodal modulation of the 18.61-year period) of different months during Pre-AAP and Post-AAP; the results are shown in Fig. 6. The model performance in terms of root mean square error (RMSE) is shown in Table 3. Figures 6a and c show that the annual amplitudes in each month at HK and CW stations were fitted well in two subperiods, and the RMSE values were generally less than 1.96 cm (Table 3). On the other hand, the model performance for the M_2 constituent significantly deteriorated at SSW station when compared with those at seaward stations (HK

Table 2. Monthly averaged tidal amplification/damping rate δ distributions for both the Pre-AAP and Post-AAP in inner (CW–SSW) and outer (HK–CW) Lingdingyang Bay and the change ratio when these two periods were compared

Season	Month	HK–CW						CW–SSW					
		Pre-AAP δ/(10^{-6} m^{-1})		Post-AAP δ/(10^{-6} m^{-1})		Ratio/%		Pre-AAP δ/(10^{-6} m^{-1})		Post-AAP δ/(10^{-6} m^{-1})		Ratio/%	
		M_2	K_1	M_2	K_1	M_2	K_1	M_2	K_1	M_2	K_1	M_2	K_1
Winter	Dec.	6.34	3.62	6.47	2.75	2.00	−24.04	3.59	1.43	3.72	1.61	3.41	12.72
	Jan.	6.59	3.31	6.60	2.76	0.02	−16.55	3.07	1.20	3.18	1.24	3.58	2.70
	Feb.	6.81	3.42	6.74	3.01	−1.04	−11.91	3.19	0.79	3.52	1.13	10.33	42.96
Spring	Mar.	7.12	3.51	6.99	3.21	−1.78	−8.41	3.21	0.32	3.68	0.90	14.65	182.12
	Apr.	7.55	3.58	7.37	3.37	−2.43	−5.88	3.09	−0.27	3.64	0.42	17.75	255.75
	May	8.06	3.63	7.82	3.45	−2.94	−4.87	2.87	−0.90	3.45	−0.20	20.24	77.71
Summer	Jun.	8.48	3.64	8.15	3.43	−3.88	−5.78	2.65	−1.36	3.25	−0.69	22.96	49.33
	Jul.	8.64	3.64	8.26	3.33	−4.48	−8.41	2.55	−1.44	3.24	−0.75	26.98	47.55
	Aug.	8.51	3.61	8.12	3.17	−4.63	−12.22	2.61	−1.07	3.41	−0.31	30.70	71.22
Autumn	Sept.	8.16	3.60	7.77	3.01	−4.81	−16.30	2.78	−0.45	3.62	0.39	30.48	186.14
	Oct.	7.66	3.59	7.36	2.88	−3.99	−19.59	3.01	0.23	3.76	0.98	25.01	334.19
	Nov.	7.05	3.59	6.92	2.80	−1.86	−21.90	3.28	0.85	3.79	1.36	15.35	59.28

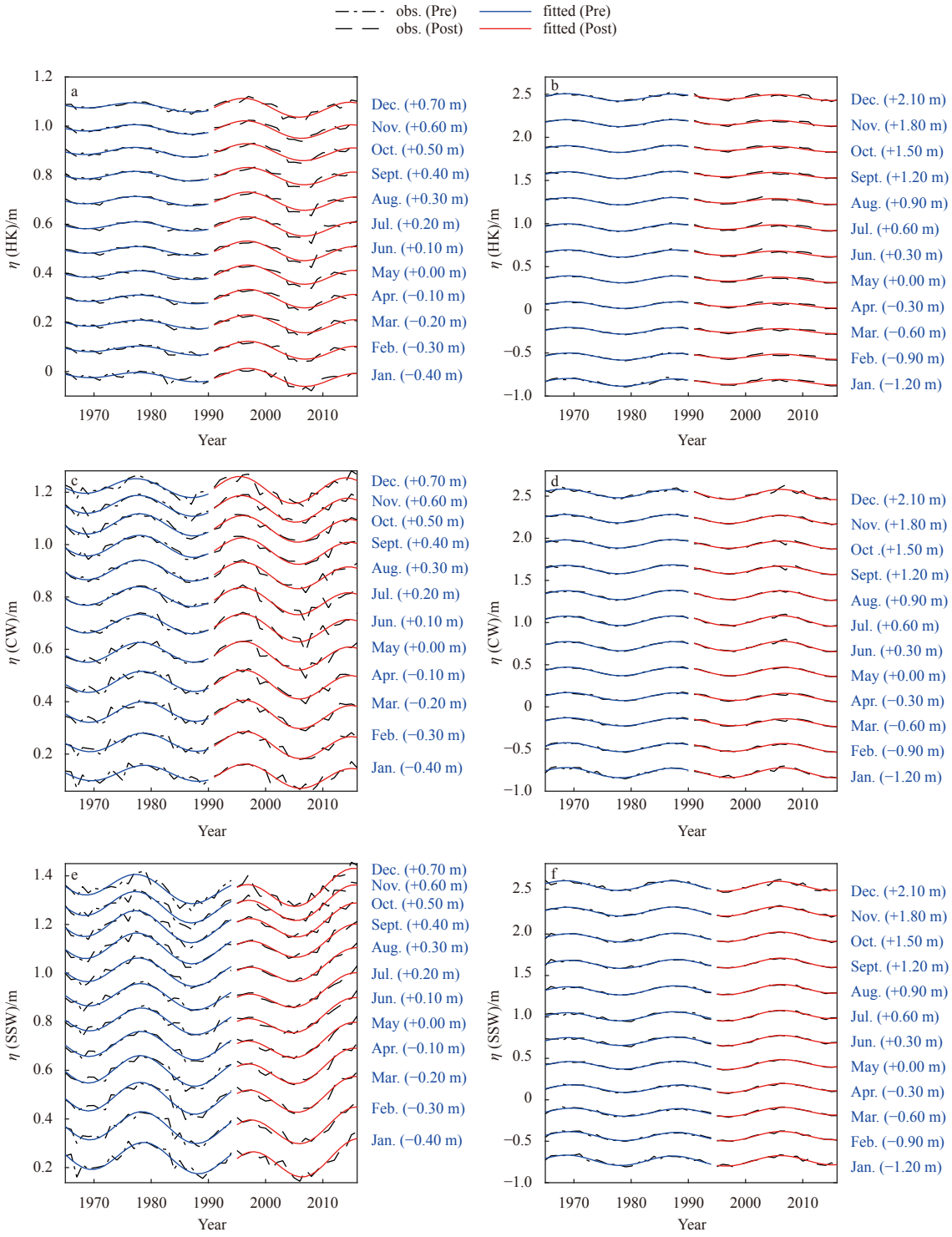

Fig. 6. Monthly averaged M_2 (a, b, e) and K_1 (c, d, f) tidal amplitudes at HK (a, b), CW (c, d), and SSW (e, f) stations from 1965 to 2016 during Pre-AAP and Post-AAP. Black dashed lines present monthly averaged values obtained from the EHA model. Red solid lines are the best-fitted curves of the 18.61-year lunar nodal modulation.

and CW stations) during Pre-AAP. Thus, the RMSE values for the M_2 constituent were larger at SSW station (less than 1.39 cm) than those at HK and CW stations (Table 3). However, during Post-AAP, the model fitted worst in CW station for M_2 constituent. In particular, after human interventions, the RMSE values were generally increased in HK and CW stations while it was opposite in SSW station. For the K_1 constituent, the regression model performance was good in all HK, CW, and SSW stations and the RMSE values were generally less than 1.96 cm.

To identify the seasonal variations of the linear trend and nodal modulation at HK, CW, and SSW stations, this study extracted the linear trend parameters β_1 and β_2 (see their definitions in Eq. (5)) of M_2 and K_1 constituents and the results are shown in Fig. 7. Figures 7a and b show the seasonality of β_1 in

Table 3. Model performance in terms of RMSE for fitting M_2 and K_1 tidal amplitudes of 18.61-year nodal modulation at HK, CW, and SSW stations from 1965 to 2016 during Pre-AAP and Post-AAP

Month	RMSE/cm											
	M_2						K_1					
	HK		CW		SSW		HK		CW		SSW	
	Pre-AAP	Post-AAP	Pre-AAP	Post-AAP	Pre-AAP	Post-AAP	Pre-AAP	Post-AAP	Pre-AAP	Post-AAP	Pre-AAP	Post-AAP
Jan.	1.02	1.16	1.21	1.26	1.52	1.39	1.36	1.41	1.75	1.53	1.90	1.36
Feb.	0.69	0.71	1.02	1.17	1.26	0.80	0.98	0.86	1.51	1.02	1.36	0.72
Mar.	0.59	0.55	0.99	1.20	1.42	0.75	0.97	1.13	1.53	1.00	1.34	0.74
Apr.	0.57	0.43	0.95	1.25	1.34	0.73	1.09	0.95	1.32	0.77	1.29	0.73
May	0.53	0.34	0.98	1.41	0.99	0.54	1.40	0.48	1.04	0.70	1.11	0.54
Jun.	0.53	0.51	1.14	1.63	0.85	0.63	1.72	0.90	1.16	1.23	1.11	0.65
Jul.	0.49	0.53	1.23	1.62	0.75	0.72	1.63	0.87	1.18	1.29	1.03	0.72
Aug.	0.42	0.46	1.15	1.37	0.62	0.68	1.24	0.69	1.02	0.97	0.81	0.62
Sept.	0.47	0.57	1.04	1.17	0.88	0.75	1.02	1.31	1.20	1.08	0.86	0.65
Oct.	0.49	0.53	0.93	1.12	1.03	0.74	0.95	1.35	1.39	1.03	1.03	0.69
Nov.	0.42	0.47	0.89	1.24	0.97	0.79	1.01	0.87	1.43	0.73	1.30	0.93
Dec.	0.56	1.02	1.13	1.65	1.29	1.38	1.64	1.91	1.79	1.66	1.96	1.70
AVG	0.56	0.61	1.06	1.34	1.08	0.83	1.25	1.06	1.36	1.08	1.26	0.84

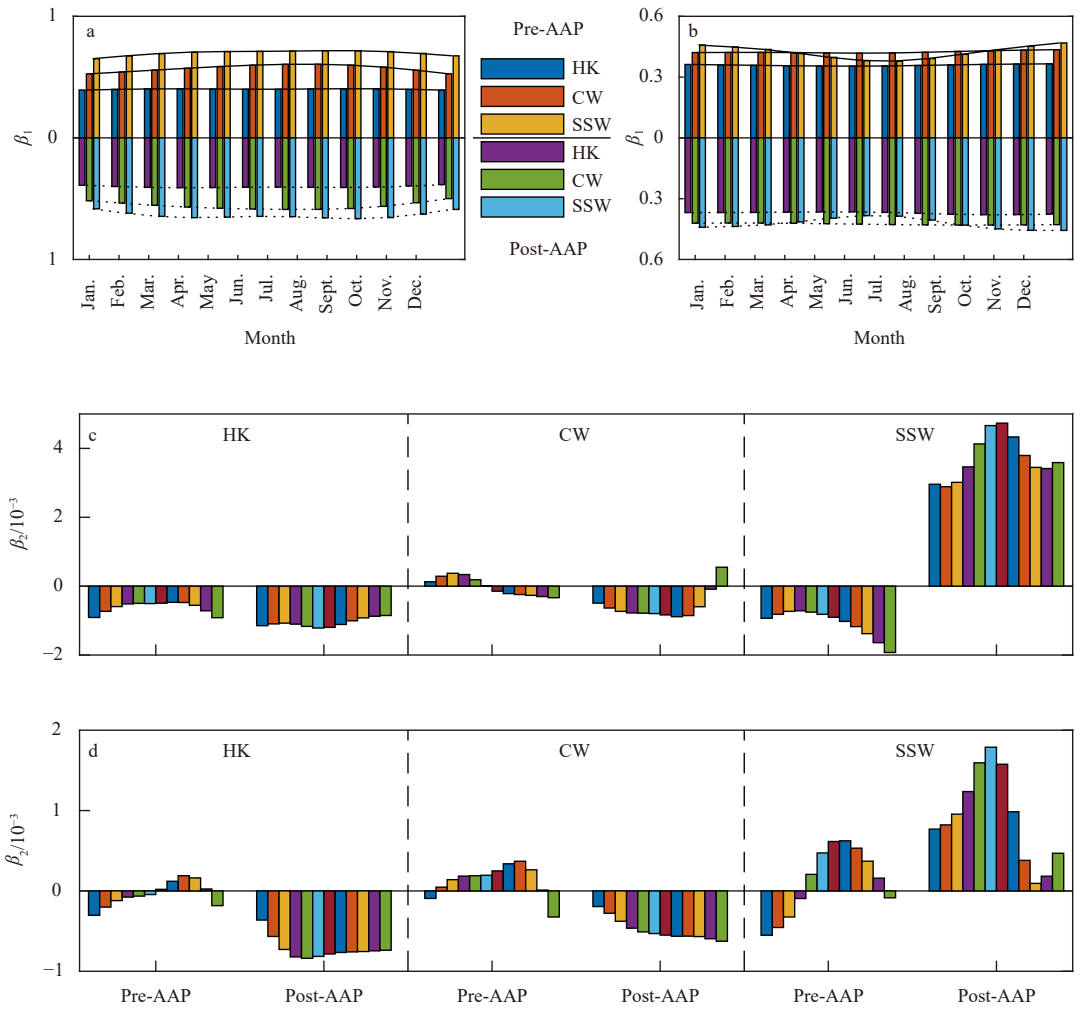

Fig. 7. Monthly averaged alterations in linear nodal parameters β_1 (a, b) and β_2 (c, d) for M_2 (a, c) and K_1 (b, d) constituents at HK, CW, and SSW stations during Pre-AAP and Post-AAP.

three stations for M_2 and K_1 constituents performed similarly during both Pre-AAP and Post-AAP, which indicates that human interventions had limited impact on β_1. Concerning the seasonal variation of β_2, Fig. 7c shows that the values of β_2 had various performances in different stations during Pre-AAP and Post-AAP. To be more specific, for the M_2 constituent, the values of β_2 were

negative at HK in two sub-periods, with the absolute minimum value during Pre-AAP occurred in June (-0.506×10^{-3}) while it occurred in June (-1.215×10^{-3}) during Post-AAP. In CW station, the values of β_2 changed from positive to negative after July in Pre-AAP, while those were negative values during Post-AAP except December. The values of β_2 were all negative during Pre-AAP in SSW station, among which the absolute maximum value occurred in December (-1.927×10^{-3}), while those were positive during Post-AAP and the maximum one occurred in July (4.733×10^{-3}). A similar pattern can also be observed from Fig. 7d that the influence of human interventions affected most heavily in the landward station (SSW) for the linear trend of 18.61-year nodal modulation for the K_1 constituent.

Subsequently, this study extracted the amplitudes of the 18.61-year lunar nodal modulation and defined R as the ratio of the amplitude of the 18.61-year lunar nodal modulation $\eta_{18.61\text{-year}}$ to the amplitude of the M_2 or K_1 constituent during Pre-AAP and Post-AAP; the seasonal variations of the R value are shown in Fig. 8. Figures 8a and b show that the seasonal variations of $\eta_{18.61\text{-year}}$ at CW and SSW stations were stronger than HK station both for M_2 and K_1 constituents in two sub-periods. It can be seen from Fig. 8a that the minimum values of $\eta_{18.61\text{-year}}$ for M_2 constituent occurred in January (0.031 m) and July (0.050 m) in CW and SSW stations during Pre-AAP, respectively, while those both occurred in July (0.046 m in CW station, 0.047 m in SSW station) during Post-AAP. Whereas the minimum values of $\eta_{18.61\text{-year}}$ for K_1 constituent occurred in March (0.047 m during Pre-AAP and 0.044 m during Post-AAP) and April (0.046 m during Pre-AAP and 0.050 m during Post-AAP) in CW and SSW stations, respectively (Fig. 8b). In addition, the values of $\eta_{18.61\text{-year}}$ for M_2 constituents during Post-AAP in HK station were much larger than those during Pre-AAP and the seasonality became more remarkable after human interventions, but it was converse for the K_1 constituent. Simultaneously, the seasonal performance of R values for the M_2 constituent shown in Fig. 8c was equivalent with $\eta_{18.61\text{-year}}$ whose minimum values of R occurred in January and July (5.85% and 7.19%, respectively) at CW and SSW stations during Pre-AAP. But those occurred in August (7.86%) and July (6.73%), in CW and SSW stations during Post-AAP, respectively. However, during Post-AAP, the values of R in HK station were much larger and those even larger than the values in landward stations (CW and SSW stations) in June, July and August. For the K_1 constituent, the minimum values of R both occurred in March (being 10.82% and 10.88%, respectively) at HK and CW stations, respectively, while it was approximately 11.03% in SSW station (Fig. 8d). Overall, the seasonal variation of K_1 constituent was much stronger than M_2 constituent but the variation for the M_2 constituent was more significant after human interventions.

5 Discussion

5.1 *The underlying mechanism of the substantial changes in tidal amplification rate*

Many previous studies have shown that human activities resulted in considerable changes in morphology and sediment discharges in river deltas (Wang et al., 2011; Tan et al., 2016). In the Lingdingyang Bay, the human activities, such as dam construction (Liu et al., 2014; Tan et al., 2017), land reclamation, and nav-

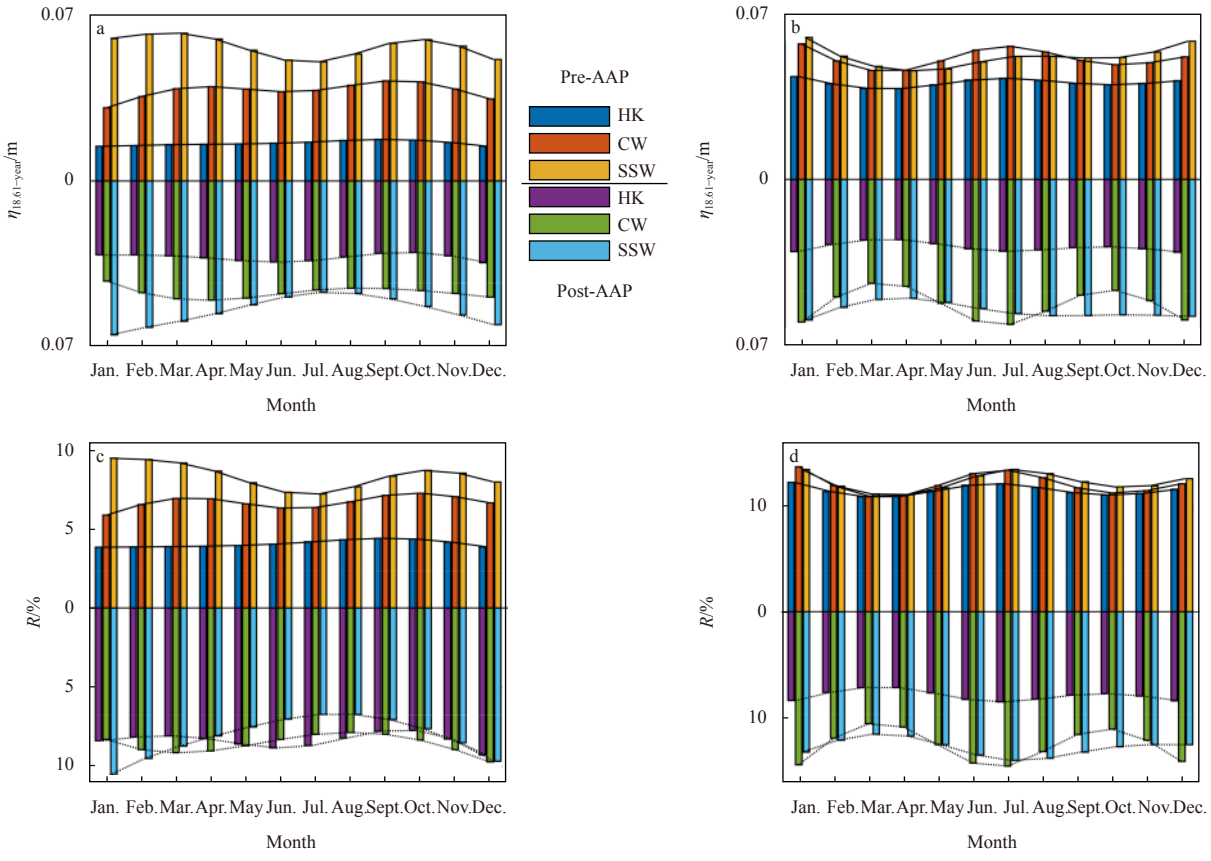

Fig. 8. The monthly averaged amplitude of 18.61-year lunar nodal modulation (a, b) and the corresponding ratio R (c, d) for M_2 (a, c) and K_1 (b, d) constituents at HK, CW and SSW stations during Pre-AAP and Post-AAP.

igational dredging in the estuary (Chen et al., 2005, 2011; Li and Damen, 2010), had significantly changed the sediment input from the river basin and altered the coastline and morphology of Lingdingyang Bay (Liu et al., 2014; Wu et al., 2014, 2016a; Zhang et al., 2015), subsequently shifted the tidal regime (Zhang et al., 2017, 2018; Mei et al., 2018; Wu et al., 2018; Talke and Jay, 2020; Wang et al., 2020b). It is worth noting that the changes in tidal hydrodynamics are also closely related to the hydraulic regime shift due to upstream river discharge and downstream sea level change conditions. However, the impacts of these two boundary conditions on tidal hydrodynamics in Lingdingyang Bay is relatively minor when compared with the dramatic change in morphology owing to the tide-dominated character of the estuarine system (Cai et al., 2020).

Channel deepening is closely related to the reduction of effective friction and strengthening of tidal dynamics (including increasing the tidal range and tidal wave celerity). Such phenomena have been observed in many estuaries worldwide, including the Thames Estuary in England (Amin, 1983), the Rhine-Meuse Estuary in the Netherlands (Vellinga et al., 2014), the Elbe and Ems Estuary in Germany, the Loire Estuary in France (Winterwerp, 2011), the Delaware, Columbia, Cape Fear, Newark, and Hudson estuaries in the United States (Familkhalili and Talke, 2016; Chant et al., 2018; Ralston et al., 2019), the Guadalquivir River Estuary in Spain (Siles-Ajamil et al., 2019), and the Modaomen Estuary in China (Cai et al., 2012). In addition, narrowing of the channel also impacts tidal hydrodynamics as it reduces the tidal prism and the tidal energy dissipation rate (Zhou et al., 2016). It has been shown that human-induced morphological changes in terms of narrowing and deepening affect the nonlinear interactions between effective hydraulic drag, fine sediment import, and tidal amplification (Winterwerp and Wang, 2013).

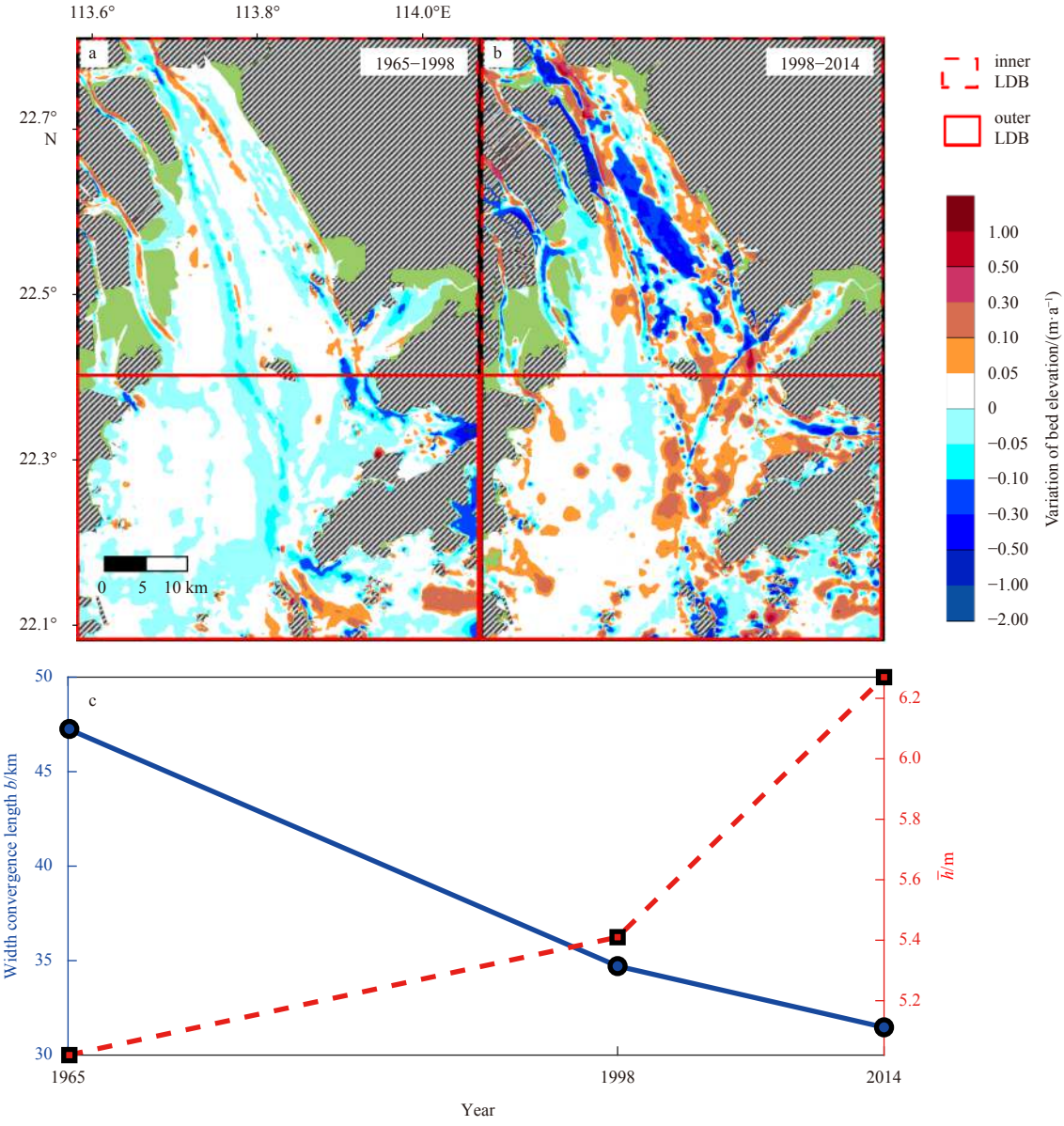

Fig. 9. Bathymetry changes of Lingdingyang Bay (LDB) from 1965 to 2014 (a. 1965–1998; b. 1998–2014) and the width convergence length b and the tidal average depth $\overline{h}$ observed in 1965, 1998, and 2014 in inner Lingdingyang Bay (c). The erosion/siltation values indicate total bathymetry change during each period and the red dashed and solid lines represent the inner and outer Lingdingyang Bay.

Table 4. The bathymetry changes in Lingdingyang Bay from 1965 to 2014 (The positive values represent siltation, while the negative values represent erosion)

Zone	Parameters	Periods	
		1965–1998	1998–2014
Inner	Volume/(10^6 m^3·a^{-1})	6.802	–51.135
	Changing rate/(m·a^{-1})	0.009	–0.021 5
Outer	Volume/(10^6 m^3·a^{-1})	0.855	70.781
	Changing rate/(m·a^{-1})	0.001	0.027

Previous studies have shown that both channel deepening and narrowing caused by large-scale human interventions have dramatically altered the morphology in Lingdingyang Bay (e.g., Wu et al., 2014, 2016a, b), which substantially enlarged the bay volume and reduced the effective bottom friction, resulting in faster wave celerity and stronger wave amplification (e.g., Cai et al., 2020; Wang et al., 2020b).

To further understand the underlying mechanism of tidal hydrodynamics changes, this study explored the changes in erosion and siltation patterns in both inner and outer Lingdingyang Bay and the results were shown in Fig. 9 and Table 4. Figure 9 shows the bathymetry changes of Lingdingyang Bay in 1965–2014 with the positive variation of bed elevation representing the siltation, otherwise representing the erosion. It is clearly shown in Fig. 9a that the siltation dominated in the inner and outer Lingdingyang Bay during 1965–1998. Specifically, the siltation in inner Lingdingyang Bay was greater than that in outer Lingdingyang Bay, with a siltation volume of 6.802×10^6 m^3/a and 0.855×10^6 m^3/a, respectively (Table 4). In addition, it can be seen from Table 4 that the elevation changing rate in inner Lingdingyang Bay was about 0.009 m/a, which was nine times larger than that in outer Lingdingyang Bay (0.001 m/a). The deepening in inner and outer Lingdingyang Bay might cause stronger tidal hydrodynamics. During 1998–2014, the siltation pattern in inner Lingdingyang Bay turned into erosion, with a significant erosion volume of 51.135×10^6 m^3/a, while it remained siltation pattern in outer Lingdingyang Bay, with a siltation volume of 70.781×10^6 m^3/a. Table 4 also shows that the elevation changing rate in inner Lingdingyang Bay was approximately 0.027 m/a while that was about –0.021 5 m/a in outer Lingdingyang Bay, which is mainly due to the channel dredging and sand excavation. Overall, the impacts of human-induced morphological changes were more significant in inner Lingdingyang Bay than those in outer Lingdingyang Bay, which caused a stronger change of tidal hydrodynamics in inner Lingdingyang Bay.

To illustrate the alteration in morphological changes in inner Lingdingyang Bay, this study assumed that the tidally averaged cross-sectional area $\overline{A}$ and width $\overline{B}$ can be approximated by the following exponential functions:

$$\overline{A} = \overline{A_0}\exp\left(-\frac{x}{a}\right), \tag{10}$$

$$\overline{B} = \overline{B_0}\exp\left(-\frac{x}{b}\right), \tag{11}$$

where x is the longitudinal coordinate directed landward, $\overline{A_0}$ and $\overline{B_0}$ represent the corresponding values at the estuary mouth, and a and b are the convergence lengths of the cross-sectional area and width, respectively. Subsequently, the tidally average depth is determined by $\overline{h} = \overline{A}/\overline{B}$ based on the assumption of the most rectangular cross-section. Figure 9c shows that the width convergence length b showed a decreasing trend by approximately 15.79 km, while the spatially tidally averaged depth $\overline{h}$ displayed an increasing trend by 1.25 m, which suggests that both geometric parameters were dramatically changed.

Many previous studies have shown that the tidal regime shift is caused by the channel deepening and narrowing, which substantially reduced effective bottom friction and led to stronger amplification and faster tidal wave celerity (Cai et al., 2020; Wang et al., 2020b). Here, Eq. (5) was used to illustrate the influence of human intervention on tidal amplification rate. Four parameters (β_1, β_2, α_1 and α_2) were calculated by using Eq. (5) to match the observed amplitude of the M_2 constituent during the Pre-AAP (1965–1990 in outer Lingdingyang Bay; 1965–1994 in inner Lingdingyang Bay) and then used the four calibrated parameters to estimate the amplitude during the Post-AAP (1991–2016 in outer Lingdingyang Bay; 1995–2016 in inner Lingdingyang Bay) in January (Figs 10a, c and e) and July (Figs 10b, d and f), respectively. Subsequently, the same approach was used to fit the observed amplitude of the M_2 constituent during the Post-AAP. The observed amplitudes of the M_2 constituent at HK station during the Post-AAP were clearly larger than those predicted using the calibrated parameters for the Pre-AAP, whereas the opposite was observed at CW station. Therefore, the gap between upstream (CW) to the downstream station (HK) became smaller, explaining the main reason for the substantial decrease in tidal amplification in outer Lingdingyang Bay. On the contrary, the observed amplitudes of the M_2 constituent at CW station during the Post-AAP were clearly smaller than those predicted using the calibrated parameters for the Pre-AAP, whereas the opposite was observed at SSW station. This was the main reason for the substantial increase in tidal amplification in inner Lingdingyang Bay since the gap between the upstream (SSW) to the downstream station (CW) became smaller. A similar picture for the K_1 constituent can be observed in Fig. S1 (see the Supplementary information). It is worth noting that the current analyses for tidal hydrodynamics mainly focused on the East Channel since the adopted three gauging stations all situated along the east side of the Lingdingyang Bay, thus further studies on tidal hydrodynamics for the whole Lingdingyang Bay are required making use of detailed numerical simulations in the future.

5.2 *Evolution in the relationship between c and δ in inner Lingdingyang Bay*

It is worth exploring the relationship between the tidal wave celerity c and the tidal damping/amplification rate δ, which is an effective predictor for quantifying the tidal regime shift in inner Lingdingyang Bay. Here the formula was adapted for the tidally averaged depth $\overline{h}$ in terms of the width convergence length b, tidal wave celerity c, and tidal amplification/damping rate δ derived by Cai et al. (2020):

$$\overline{h} = \frac{r_s b c^2 \omega^2}{g(\delta c^2 - \delta^2 c^2 b + b\omega^2)}, \tag{12}$$

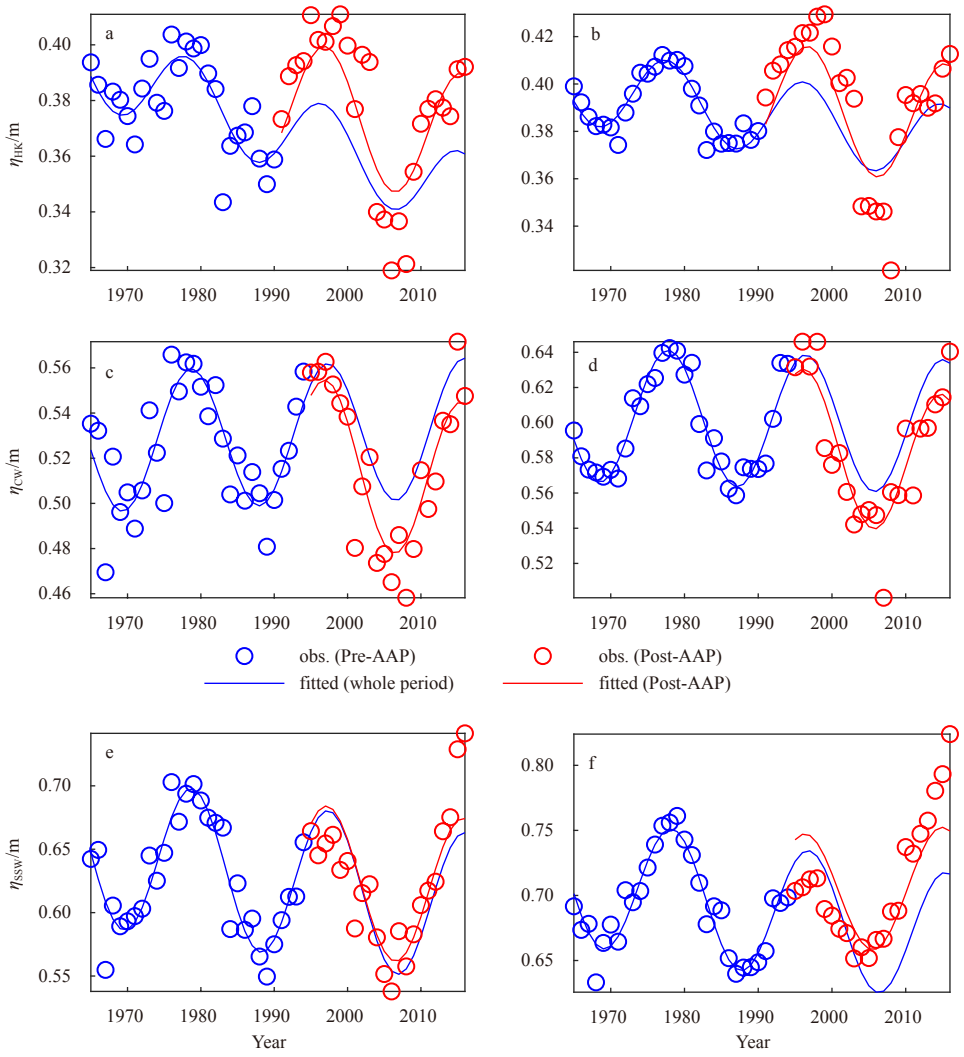

Fig. 10. Time series of tidal amplitudes of the M_2 constituent in January (a, c, e) and July (b, d, f) at HK (a, b), CW (c, d), and SSW (e, f) stations. Blue and red hollow cycles represent the harmonic results during the Pre-AAP and the Post-AAP, respectively. Blue solid lines represent the best-fitted curves of 18.61-year lunar nodal modulation for the whole study period using the calibrated parameters for the Pre-AAP. Red solid lines represent the best-fitted curves of 18.61-year lunar nodal modulation for the Post-AAP.

where r_s is the storage width ratio accounting for the possible dynamic effect from the lateral storage area (e.g., tidal flats), g is the gravitational acceleration. After some algebraic manipulations, Eq. (9) can be rearranged as an empirical formula linking the square of tidal wave celerity c^2 to the tidal amplification/damping rate δ:

$$c^2 = \frac{\overline{h}gb\omega^2}{\overline{h}gb\delta^2 - \overline{h}g\delta + r_s b\omega^2}. \tag{13}$$

Figure 11 shows the variations of the square of the tidal wave celerity c^2 as a function of the tidal amplification/damping rate δ in the two different periods and the fitting results were presented in Table 5. Here, based on the comparison of the observed and fitted value of c^2 obtained from Eq. (13), the calibrated parameter r_s in Pre-AAP (1.03) and Post-AAP (1.19) were obtained. The r_s values were subsequently used to calculate the fitted value of width convergence length b and tidally averaged depth $\overline{h}$. This study observe that the fitted results of b and $\overline{h}$ were different from the actual values in inner Lingdingyang Bay (Fig. 9c), but the tendencies were consistent. The derivation is mainly due to the highly sensitivity of the square of wave celerity with regard to these two geometric parameters (Eq. (13)). It can be seen from Fig. 11a that the square of the tidal wave celerity c^2 remained more or less constant with the increase of the tidal amplification/damping rate δ during the Pre-AAP for the M_2 constituent, while the values of c^2 were considerably increased with the δ during the Post-AAP. By contrast, for the K_1 constituent, the values of c^2 increased with the δ for both the Pre-AAP and Post-AAP (Fig. 11b), with a larger increasing rate during the Post-AAP than that during the Pre-AAP. It can be observed in Table 5 that the fitted width convergence length b decreased from the Pre-AAP to Post-AAP for both M_2 and K_1 constituents, while the tidal average depth $\overline{h}$ increased, which suggests a dramatic effect of channel narrowing and deepening on the tidal hydrodynamics in inner Lingdingyang Bay.

6 Conclusions

In this study, the EHA method was adopted to quantify the

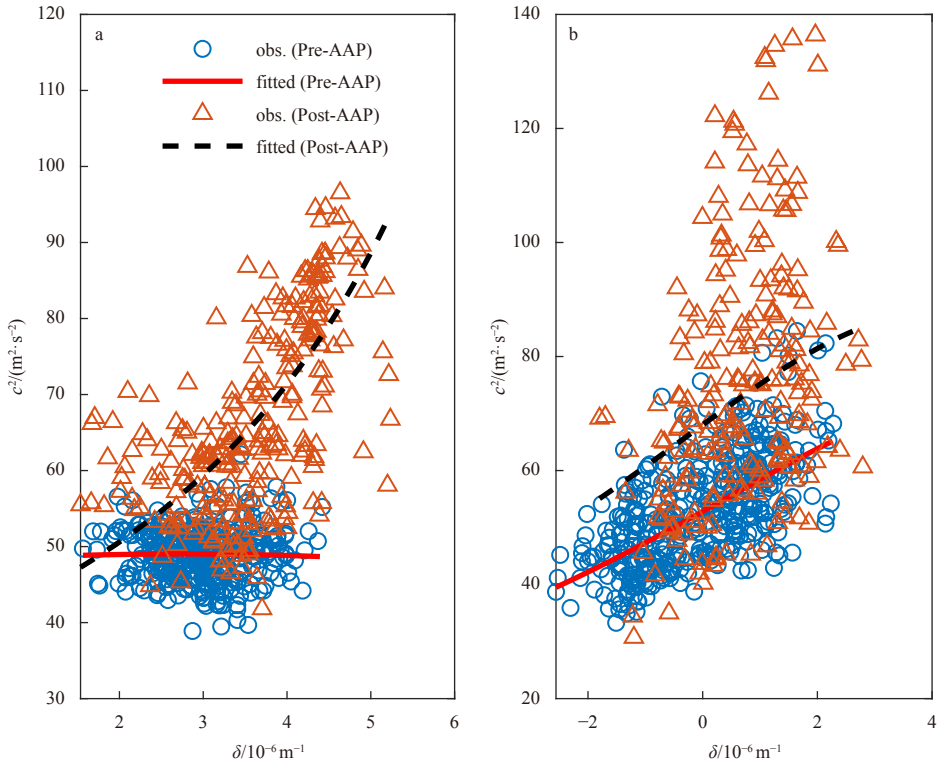

Fig. 11. The variations of the square of the monthly averaged tidal wave celerity c^2 as a function of the tidal amplification/damping rate δ for M_2 (a) and K_1 (b) constituents during the Pre-AAP and Post-AAP in inner Lingdingyang Bay.

Table 5. Fitting results of width convergence length b and tidally averaged depth $\overline{h}$ for M_2 and K_1 by means of the square of the tidal wave celerity c^2 as a function of the tidal amplification/damping rate δ during the Pre-AAP and Post-AAP in inner Lingdingyang Bay

Periods	M_2		K_1	
	b/km	$\overline{h}$/m	b/km	$\overline{h}$/m
Pre-AAP	130.80	4.89	112.12	5.51
Post-AAP	15.92	4.98	42.61	7.41

seasonal variability of tidal hydrodynamics in terms of tidal wave celerity and the tidal amplification/damping rate in inner and outer Lingdingyang Bay of the ZRD. To highlight the impacts of human interventions (e.g., dredging for navigational channels and land reclamation) on tidal hydrodynamics, the whole study period was divided into two distinct periods, including the Pre-AAP (1965–1990 for outer Lingdingyang Bay, 1965–1994 for inner Lingdingyang Bay, respectively) and the Post-AAP (1991–2016 for outer Lingdingyang Bay and 1995–2016 for inner Lingdingyang Bay, respectively), based on the accumulated anomaly curve of the monthly averaged tidal wave celerity time series for the M_2 constituent. Observations showed that the tidal wave celerity c was considerably increased (for M_2 and K_1 constituents, by 34.15% and 22.67%, respectively) but tidal amplification/damping rate δ considerably decreased (for M_2 and K_1 constituent, by -2.49% and –12.99% on average, respectively) in outer Lingdingyang Bay from the Pre-AAP to the Post-AAP. For inner Lingdingyang Bay, both the tidal wave celerity c and tidal amplification/damping rate δ were considerably increased (for the M_2 constituent, by 15.30% and 18.45% on average, respectively; for the K_1 constituent, by 15.44% and 110.14% on average, respectively) from the Pre-AAP to the Post-AAP. In addition, results from the regression model accounting for the 18.61-year lunar nodal modulation suggest that the minimum values of $\eta_{18.61\text{-year}}$ for the M_2 constituent occurred in January (0.036 m) and July (0.046 m) in CW and SSW stations, respectively, while those for the K_1 constituent occurred in March (0.045 m) and April (0.048 m), respectively. Overall, the effects of human interventions on seasonal dynamics for the K_1 constituent were much stronger than those for the M_2 constituent. The substantial decrease in tidal amplification in outer Lingdingyang Bay was shown to be related to the larger increase of the M_2 and K_1 amplitudes at HK station and smaller values at CW station while it was a contrast in inner Lingdingyang Bay, which associates with strong interventions from human activities (e.g., dredging for navigational channels and land reclamation). Overall, the variations in inner Lingdingyang Bay were larger than those in outer Lingdingyang Bay. The results obtained from this study are particularly useful for setting scientific guidelines for sustainable water resources management in Lingdingyang Bay and other estuaries with substantial human interventions.

Acknowledgements

The S_TIDE toolbox can be freely accessed via the following link: https://www.researchgate.net/project/A-non-stationary-tidal-analysis-toolbox-S-TIDE.

References

Amin M. 1983. On perturbations of harmonic constants in the Thames Estuary. Geophysical Journal International, 73(3): 587–603, doi: 10.1111/j.1365-246x.1983.tb03334.x

Cai Huayang, Savenije H H G, Jiang Chenjuan, et al. 2016. Analytical approach for determining the mean water level profile in an estuary with substantial fresh water discharge. Hydrology and

Earth System Sciences, 20(3): 1177–1195, doi: 10.5194/hess-20-1177-2016

Cai Huayang, Savenije H H G, Yang Qingshu, et al. 2012. Influence of river discharge and dredging on tidal wave propagation: modaomen estuary case. Journal of Hydraulic Engineering, 138(10): 885–896, doi: 10.1061/(asce)hy.1943-7900.0000594

Cai Huayang, Zhang Ping, Garel E, et al. 2020. A novel approach for the assessment of morphological evolution based on observed water levels in tide-dominated estuaries. Hydrology and Earth System Sciences, 24(4): 1871–1889, doi: 10.5194/hess-24-1871-2020

Caldwell P C, Merrifield M A, Thompson P R. 2015. Sea Level Measured by Tide Gauges from Global Oceans—the Joint Archive for Sea Level holdings (NCEI Accession 0019568), Version 5.5. Honolulu, HI, USA: NOAA National Centers for Environmental Information, Dataset, doi: 10.7289/V5V40S7W

Chant R J, Sommerfield C K, Talke S A. 2018. Impact of channel deepening on tidal and gravitational circulation in a highly engineered estuarine basin. Estuaries and Coasts, 41(6): 1587–1600, doi: 10.1007/s12237-018-0379-6

Chen Shuisen, Chen Liangfu, Liu Qinhuo, et al. 2005. Remote sensing and GIS-based integrated analysis of coastal changes and their environmental impacts in Lingding Bay, Pearl River Estuary, South China. Ocean & Coastal Management, 48(1): 65–83

Chen Xiaowen, Liu Xia, Zhang Wei. 2011. Shore reclamation in Pearl River esturay and its impact analysis. Journal of Hohai University (Natural Sciences) (in Chinese), 39(1): 39–43

Corkan R H. 1934. An annual perturbation in the range of tide. Proceedings of the Royal Society A: Mathematical, Physical and Engineering Sciences, 144(853): 537–559, doi: 10.1098/rspa.1934.0067

Devlin A T, Jay D A, Talke S A, et al. 2014. Can tidal perturbations associated with sea level variations in the western Pacific Ocean be used to understand future effects of tidal evolution?. Ocean Dynamics, 64(8): 1093–1120, doi: 10.1007/s10236-014-0741-6

Devlin A T, Jay D A, Talke S A, et al. 2017. Tidal variability related to sea level variability in the Pacific Ocean. Journal of Geophysical Research: Oceans, 122(11): 8445–8463, doi: 10.1002/2017JC013165

Devlin A T, Zaron E D, Jay D A, et al. 2018. Seasonality of tides in southeast Asian waters. Journal of Physical Oceanography, 48(5): 1169–1190, doi: 10.1175/JPO-D-17-0119.1

Familkhalili R, Talke S A. 2016. The effect of channel deepening on tides and storm surge: a case study of Wilmington, NC. Geophysical Research Letters, 43(17): 9138–9147, doi: 10.1002/2016GL069494

Feng Xiangbo, Tsimplis M N, Woodworth P L. 2015. Nodal variations and long-term changes in the main tides on the coasts of China. Journal of Geophysical Research: Oceans, 120(2): 1215–1232, doi: 10.1002/2014JC010312

Godin G. 1985. Modification of river tides by the discharge. Journal of Waterway, Port, Coastal, and Ocean Engineering, 111(2): 257–274, doi: 10.1061/(ASCE)0733-950X(1985)111:2(257)

Godin G. 1999. The propagation of tides up rivers with special considerations on the upper Saint Lawrence river. Estuarine, Coastal and Shelf Science, 48(3): 307–324, doi: 10.1006/ecss.1998.0422

Gräwe U, Burchard H, Müller M, et al. 2014. Seasonal variability in M_2 and M_4 tidal constituents and its implications for the coastal residual sediment transport. Geophysical Research Letters, 41(15): 5563–5570, doi: 10.1002/2014GL060517

Guo Leicheng, van der Wegen M, Jay D A, et al. 2015. River-tide dynamics: exploration of nonstationary and nonlinear tidal behavior in the Yangtze River estuary. Journal of Geophysical Research, 120(5): 3499–3521, doi: 10.1002/2014JC010491

Huess V, Andersen O B. 2001. Seasonal variation in the main tidal constituent from altimetry. Geophysical Research Letters, 28(4): 567–570, doi: 10.1029/2000gl011921

Jin Guangzhen, Pan Haidong, Zhang Qilin, et al. 2018. Determination of harmonic parameters with temporal variations: an enhanced harmonic analysis algorithm and application to internal tidal currents in the South China Sea. Journal of Atmospheric and Oceanic Technology, 35(7): 1375–1398, doi: 10.1175/JTECH-D-16-0239.1

Kang S K, Chung J Y, Lee S R, et al. 1995. Seasonal variability of the M_2 tide in the seas adjacent to Korea. Continental Shelf Research, 15(9): 1087–1113, doi: 10.1016/0278-4343(94)00066-V

Li Xuejie, Damen M C J. 2010. Coastline change detection with satellite remote sensing for environmental management of the Pearl River Estuary, China. Journal of Marine Systems, 82(S1): S54–S61, doi: 10.1016/j.jmarsys.2010.02.005

Liu Feng, Yuan Lirong, Yang Qingshu, et al. 2014. Hydrological responses to the combined influence of diverse human activities in the Pearl River delta, China. CATENA, 113: 41–55, doi: 10.1016/j.catena.2013.09.003

Mao Qingwen, Shi Ping, Yin Kedong, et al. 2004. Tides and tidal currents in the Pearl River Estuary. Continental Shelf Research, 24(16): 1797–1808, doi: 10.1016/j.csr.2004.06.008

Mei Xuefei, Dai Zhijun, Wei Wen, et al. 2018. Secular bathymetric variations of the North Channel in the Changjiang (Yangtze) Estuary, China, 1880–2013: causes and effects. Geomorphology, 303: 30–40, doi: 10.1016/j.geomorph.2017.11.014

Müller M. 2012. The influence of changing stratification conditions on barotropic tidal transport and its implications for seasonal and secular changes of tides. Continental Shelf Research, 47: 107–118, doi: 10.1016/j.csr.2012.07.003

Müller M, Cherniawsky J Y, Foreman M G G, et al. 2014. Seasonal variation of the M_2 tide. Ocean Dynamics, 64(2): 159–177, doi: 10.1007/s10236-013-0679-0

Pan Haidong, Guo Zheng, Wang Yingying, et al. 2018a. Application of the EMD method to river tides. Journal of Atmospheric and Oceanic Technology, 35(4): 809–819, doi: 10.1175/JTECH-D-17-0185.1

Pan Haidong, Lv Xianqing, Wang Yingying, et al. 2018b. Exploration of tidal-fluvial interaction in the Columbia River Estuary using S_TIDE. Journal of Geophysical Research: Oceans, 123(9): 6598–6619, doi: 10.1029/2018JC014146

Pan Haidong, Zheng Quanxin, Lv Xianqing. 2019. Temporal changes in the response of the nodal modulation of the M_2 tide in the Gulf of Maine. Continental Shelf Research, 186: 13–20, doi: 10.1016/j.csr.2019.07.007

Pawlowicz R, Beardsley B, Lentz S. 2002. Classical tidal harmonic analysis including error estimates in MATLAB using T_TIDE. Computers & Geosciences, 28(8): 929–937, doi: 10.1016/s0098-3004(02)00013-4

Pugh D, Woodworth P. 2014. Sea-level Science: Understanding Tides, Surges, Tsunamis and Mean Sea-Level Changes. Cambridge, UK: Cambridge University Press, 395

Ralston D K, Talke S, Geyer W R, et al. 2019. Bigger tides, less flooding: effects of dredging on barotropic dynamics in a highly modified estuary. Journal of Geophysical Research: Oceans, 124(1): 196–211, doi: 10.1029/2018JC014313

Siles-Ajamil R, Díez-Minguito M, Losada M Á. 2019. Tide propagation and salinity distribution response to changes in water depth and channel network in the Guadalquivir River Estuary: an exploratory model approach. Ocean & Coastal Management, 174: 92–107, doi: 10.1016/j.ocecoaman.2019.03.015

St-Laurent P, Saucier F J, Dumais J F. 2008. On the modification of tides in a seasonally ice-covered sea. Journal of Geophysical Research: Oceans, 113(C11): C11014, doi: 10.1029/2007JC004614

Talke S A, Jay D A. 2020. Changing tides: the role of natural and anthropogenic factors. Annual Review of Marine Science, 12: 121–151, doi: 10.1146/annurev-marine-010419-010727

Tan Chao, Huang Bensheng, Liu Feng, et al. 2016. Transformation of the three largest Chinese river deltas in response to the reduction of sediment discharges. Journal of Coastal Research, 32(6): 1402–1416, doi: 10.2112/jcoastres-d-15-00007.1

Tan Chao, Huang Bensheng, Liu Kunsong, et al. 2017. Using the wavelet transform to detect temporal variations in hydrological processes in the Pearl River, China. Quaternary International, 440: 52–63, doi: 10.1016/j.quaint.2016.02.043

Tazkia A R, Krien Y, Durand F, et al. 2017. Seasonal modulation of M_2

tide in the Northern Bay of Bengal. Continental Shelf Research, 137: 154–162, doi: 10.1016/j.csr.2016.12.008
Vellinga N E, Hoitink A J F, van der Vegt M, et al. 2014. Human impacts on tides overwhelm the effect of sea level rise on extreme water levels in the Rhine–Meuse Delta. Coastal Engineering, 90: 40–50, doi: 10.1016/j.coastaleng.2014.04.005
Wang Daosheng, Pan Haidong, Jin Guangzhen, et al. 2020a. Seasonal variation of the principal tidal constituents in the Bohai Sea. Ocean Science, 16(1): 1–14, doi: 10.5194/os-16-1-2020
Wang Houjie, Saito Y, Zhang Yong, et al. 2011. Recent changes of sediment flux to the western Pacific Ocean from major rivers in East and Southeast Asia. Earth-Science Reviews, 108(1–2): 80–100, doi: 10.1016/j.earscirev.2011.06.003
Wang Heng, Zhang Ping, Hu Shuai, et al. 2020b. Tidal regime shift in Lingdingyang Bay, the Pearl River Delta: an identification and assessment of driving factors. Hydrological Processes, 34(13): 2878–2894, doi: 10.1002/hyp.13773
Wei Fengying. 2007. Climatological Statistical Diagnosis and Prediction Technology (in Chinese). Beijing: China Meteorological Press, 62
Winterwerp J C. 2011. Fine sediment transport by tidal asymmetry in the high-concentrated Ems River: indications for a regime shift in response to channel deepening. Ocean Dynamics, 61(2–3): 203–215, doi: 10.1007/s10236-010-0332-0
Winterwerp J C, Wang Zhengbing. 2013. Man-induced regime shifts in small estuaries: I. theory. Ocean Dynamics, 63(11–12): 1279–1292, doi: 10.1007/s10236-013-0662-9
Wu Ziyin, Milliman J D, Zhao Dineng, et al. 2014. Recent geomorphic change in Lingding Bay, China, in response to economic and urban growth on the Pearl River Delta, Southern China. Global and Planetary Change, 123: 1–12, doi: 10.1016/j.gloplacha.2014.10.009
Wu Ziyin, Milliman J D, Zhao Dineng, et al. 2018. Geomorphologic changes in the lower Pearl River Delta, 1850–2015, largely due to human activity. Geomorphology, 314: 42–54, doi: 10.1016/j.geomorph.2018.05.001
Wu Ziyin, Saito Y, Zhao Dineng, et al. 2016a. Impact of human activities on subaqueous topographic change in Lingding Bay of the Pearl River Estuary, China, during 1955–2013. Scientific Reports, 6(1): 37742, doi: 10.1038/srep37742
Wu Chuangshou, Yang Shilun, Huang Shichang, et al. 2016b. Delta changes in the Pearl River Estuary and its response to human activities (1954–2008). Quaternary International, 392: 147–154, doi: 10.1016/j.quaint.2015.04.009
Ye L, Preiffer K D. 1990. Studies of 2D & 3D numerical simulation of Kelvin tide wave in Nei Lingdingyang at Pearl River Estuary. Ocean Engineering, 8(4): 33–44
Zhang Wei, Cao Yu, Zhu Yuliang, et al. 2017. Flood frequency analysis for alterations of extreme maximum water levels in the Pearl River Delta. Ocean Engineering, 129: 117–132, doi: 10.1016/j.oceaneng.2016.11.013
Zhang Wei, Cao Yu, Zhu Yuliang, et al. 2018. Unravelling the causes of tidal asymmetry in deltas. Journal of Hydrology, 564: 588–604, doi: 10.1016/j.jhydrol.2018.07.023
Zhang Wei, Xu Yang, Hoitink A J F, et al. 2015. Morphological change in the Pearl River Delta, China. Marine Geology, 363: 202–219, doi: 10.1016/j.margeo.2015.02.012
Zhou Qing, Gong Qinghua, Sun Zhongyu, et al. 2016. Long-term geomorphic changes in the coastal profile of Lingding Bay in the Pearl River Estuary and the response to tides since 1906. Journal of Disaster Research, 11(5): 995–1002, doi: 10.20965/jdr.2016.p0995

Supplementary information:

Fig. S1. Time series of tidal amplitude of the K_1 constituent in January (a, c, e) and July (b, d, f) at HK (a, b), CW (c, d) and SSW (e, f) stations. Blue and red hollow cycles represent the harmonic results during the Pre-AAP and the Post-AAP, respectively. Blue solid lines represent the best fitted curves of 18.61-year lunar nodal modulation for the whole study period using the calibrated parameters for the Pre-AAP. Red solid lines represent the best fitted curves of 18.61-year lunar nodal modulation for the Post-AAP.

The supplementary information is available online at https://10.1007/s13131-021-1831-1 and www.aosocean.com. The supplementary information is published as submitted, without typesetting or editing. The responsibility for scientific accuracy and content remains entirely with the authors.